

Minkowski Functionals: An MRI texture analysis tool for determination of the aggressiveness of breast Cancer

¹Mr Michael J. Fox MSc, ¹Dr Peter Gibbs PhD, ¹Dr Martin D. Pickles PhD.

¹Centre for Magnetic Resonance Investigations, HYMS at University of Hull, Hull, UK.

Corresponding Author

Michael Fox

CMRI

HYMS at University of Hull

Hull Royal Infirmary

Anlaby Road

Hull

HU3 2JZ

Email: m.fox@2013.hull.ac.uk

Telephone: +44 1482 674072

Acknowledgements

The authors would like to thank all their colleagues at the CMRI, along with Yorkshire Cancer Research for their funding of the department.

Declarations

The authors declare no conflict of interests.

Running Title

Minkowski Functionals in Breast MRI

This is the peer reviewed version of the following article: Fox, M. J., Gibbs, P. and Pickles, M. D. (2016), Minkowski functionals: An MRI texture analysis tool for determination of the aggressiveness of breast cancer. *J. Magn. Reson. Imaging*, 43: 903–910, which has been published in final form at <http://dx.doi.org/10.1002/jmri.25057>. This article may be used for non-commercial purposes in accordance With Wiley Terms and Conditions for self-archiving.

Abstract

Purpose: This work aims to see whether Minkowski Functionals can be used to distinguish between cancer types before chemotherapy treatment has begun, and whether a response to treatment can be predicted by an initial scan alone.

Methods: Fat-nulled T1w 3T DCE-MRI scans were taken of 100 cases of biopsy confirmed breast cancer and a series of binary images created on lesion containing slices. Minkowski Functionals were calculated for each binary image and the change in these values as the binary threshold was raised was described using 6th order polynomials. These polynomials were used to compare between patient sub-groups, for triple negative breast cancer (TNBC) status, chemotherapy response, biopsy grade, nodal status, and lymphovascular invasion status.

Results: When using Minkowski Functionals statistically significant ($p < 0.05$) differences were found between TNBC status, biopsy grade, and lymphovascular invasion status sub-groups for all methodologies. The analysis performance did not appear to be affected by the number of threshold steps used. Most notably, very strong differences ($p \leq 0.01$) were found between TNBC and other intrinsic subtype patients. When analysed with a binary logistic regression model, an AUC value of 0.917 (0.846 – 0.987, 95% CI) for TNBC classification was found.

Conclusion: The method of texture analysis presented here provides a novel way to characterise tumours, and demonstrates clear differences between cancer groups which are detectable before treatment begins, and can help with treatment planning as a valuable prognosis tool.

Key words: Texture analysis; breast cancer; Minkowski Functionals; contrast enhanced MRI; image processing.

Introduction

In the UK, breast cancer is the most common form of cancer in women with 49,936 new diagnoses in 2011 alone, making up 15% of all cancer cases (1). Due to increased public awareness of symptoms, improvements in detection methods, and more specialized and targeted treatment courses 5-year survival rates for breast cancer today are over 85%, a major improvement from the high mortality rates seen at the end of the 1980s (2). Unfortunately breast cancer is a heterogeneous disease presenting with varied pathological makeup and, currently, imprecise prediction of treatment response (3-6). For these reasons new detection, monitoring, and treatment methodologies are constantly being investigated to better understand and manage the disease.

Triple negative breast cancer (TNBC) is a specific sub-group of disease and carries with it known complications. The status of three receptors within a patient's tumour are tested – Estrogen (ER), Progesterone (PR), and Human epidermal growth factor (HER2) – and the combination of these statuses will determine a patient's treatment regime (7, 8). Counter-intuitively, despite the lack of targeted therapy triple negative tumours will tend to respond more readily to chemotherapy treatment due to their increased surrounding vasculature (9). Unfortunately even with the trend of a better response to chemotherapy patients with TNBC also experience higher rates of local recurrence, and ultimately a poorer prognosis (9, 10). Being able to identify patients who are triple negative early, and with higher confidence, is important to ensure they are placed on a suitable monitoring and treatment regime as early as possible.

MRI is used to detect disease, and monitor treatment response in breast cancer patients and is an invaluable tool due to its exceedingly high sensitivity – close to 100% (11, 12) – and comparable specificity rates – 70-100% (13). Image texture is commonly used to examine MR

qualitatively by eye when looking for abnormalities in morphology like level of spiculation; functionality is examined in a similar fashion by searching for higher contrast uptake areas in Dynamic Contrast Enhanced (DCE-MRI) images (14). Both of these methods are first order analysis techniques, looking simply at relative pixel intensities. Texture analysis is a quantitative method of image analysis using higher order statistics to measure the morphology of a scan by examining the distribution and/or connectivity of pixel intensities. The most common form of texture analysis utilises grey-level co-occurrence matrices (GLCM) where a scan is described using a number of parameters calculated from a matrix of counting statistics (15). Minkowski Functionals (MFs) are a novel way of describing image texture which have previously been used in computed tomography (CT) and mammography (16-18) , and have recently been used to analyse MRI images to determine malignancy (19) in the breast, and measure response to chemotherapy (20, 21).

Minkowski Functionals differ from other texture analysis techniques, as instead of examining MR scans directly they use a series of binary images created from scans using a rising threshold to remove pixels, offering an alternative method of interrogating MR images. Previous work on breast cancer using Minkowski Functionals has shown that it is possible to use them to distinguish between benign and malignant cases when used as a diagnostic tool (19), and they can also be used as a monitoring tool for chemotherapy response (20). The work presented here aims to see whether Minkowski Functionals can be used to predict response to chemotherapy treatment, and differentiate between cancer types, before the start of treatment.

Materials and Methods

Patient Cohort:

This retrospective study was cleared for ethics approval. The data was taken from 100 cases of biopsy confirmed breast cancer (98 patients, with two presenting bilaterally) before the start of

neo-adjuvant chemotherapy (NAC), between April 2006 and September 2008. The median age of the cohort was 48 (range: 31-77 years). Details of cohort statistics are presented in Table 1. Median time between pre-treatment MR scan and commencement of chemotherapy was 11.5 days (1-45 days), with the majority (59%) of patients receiving a combination of Epirubicin and Cyclophosphamide, followed by Taxotere (ECT), or a modified course of this treatment (73% including modifications).

Patients were split into sub-groups following chemotherapy to look for correlations based on five criteria. Chemotherapy response: partial responders [40] were patients with a reduction of tumour longest diameter of 50% or more, and non-responders [49] with a reduction of tumour longest diameter of less than 50% (22). Biopsy grade (23, 24): grade 1/2 [38] or grade 3 [55]. Intrinsic Subtype status (25): TNBC [22] or all other statuses [49]. Nodal status (23, 24): positive lymph node involvement [46] or negative lymph node involvement [45]. Lymphovascular invasion status (26): positive lymphovascular involvement [32], or negative lymphovascular involvement [47].

MRI Protocol:

All data was acquired using a dedicated 8-channel breast coil on a 3.0 T HDx (GE Healthcare, Milwaukee, WI) scanner. The images used for this study were obtained using a 3D dynamic contrast-enhanced (DCE) sagittal T1W fat nulled Volume Imaging for Breast Assessment (VIBRANT) sequence (10° flip angle, TR 4.1 ms, TE 1.6 ms, FOV 20x20 cm, 220x160 matrix, 4/-2 mm slice/gap). The dynamic sequence included 12 phases; 2 pre-contrast phases followed by 10 post-contrast phases with a bolus injection of gadolinium (Magnevist at 0.05 mmol/kg; Schering, Kenilworth, NJ) being added prior to the third phase, followed by a 20mL saline flush. Median temporal resolution was 33.6 s (23.5-44.6 s). Images taken from the 2nd or 3rd

post-contrast phase (whichever phase correlates to one minute post-contrast) were used for analysis to provide the greatest tumour enhancement.

Image Processing:

Software was developed in house using MatLab 2013b (Mathworks, Natick, MA) to process the images taken from the scanner and perform texture analysis. Regions of Interest (ROI) were created semi-automatically on each slice by a trained researcher using a seed point method, expanding outward to enclose the entire lesion. Images were cropped around the ROI to leave only the pixel intensities within the ROI, and a single pixel border of 0s. The median of the top and bottom 1% of pixel intensities within the ROI were then calculated and pixels with values above or below their respective median were altered to the median value. This accounted for the inclusion of any erroneous pixels which may alter counting stats in this and other forms of texture analysis. The pixels were then scaled from 0-1.

The cropped images were then converted into binary images, based on only including pixels with an intensity greater than a threshold which ranged from 0-1. By this method the first image is always set as the entire ROI as it includes all pixels above 0.0, and the final image is set as empty – as demonstrated in fig 1. For each binary image, three Minkowski Functional values are calculated to represent area (A), perimeter (U), and Euler value (χ). The three values are calculated using the equations:

$$A = n_s \quad [1]$$

$$U = -4n_s + 2n_e \quad [2]$$

$$\chi = n_s - n_e + n_v \quad [3]$$

Where n_s is given as the number of white pixels in an image, n_e the number of edges of white pixels, and n_v the number of vertices of white pixels. Examples of the counting statistics used, and corresponding MF values, are shown in fig. 2.

Three sets of threshold values were used when generating the binary images corresponding to 11, 51, and 101 processed images. These three sets were chosen to demonstrate the effect of threshold selection on analysis performance, as previous work has suggested that performance is not impeded by the number of images used (19). Before analysis, the MF values for Area and Perimeter for each binary image were scaled from 0-1 for each patient individually so as to be standardised and to represent the change in MF value as the threshold is changed. Euler values were left unaltered as they are already invariant with size. The mean MF values for each threshold level were calculated to aggregate a whole lesion across as many slices that it appears on.

Statistical Analysis:

Due to the low number of cases being used, non-parametric tests were used exclusively in the form of Mann-Whitney U-Tests to look for statistical differences between patient groups. SPSS v.20 (Chicago, IL) was used for analysis, and a p-value of 0.05 was decided as indicating a statistically significant difference.

Preliminary testing:

Mann-Whitney U-tests were used to compare between mean Minkowski Functionals for each threshold level, resulting in a total of 29 tests for each patient sub-group. Due to the large number of tests being performed on a relatively small data set, a new method of analysis was deemed necessary to reduce the possibility of type I errors.

Secondary tests:

The change in means across threshold level was then described using a polynomial fit to characterise the data; 3rd, 4th, 5th, 6th, and 7th order polynomials were tested to determine how many coefficients were necessary to accurately describe, but not over fit, the change in MF values. U-tests were then conducted comparing the values of each term of the polynomial to find differences in the shape of the change of means as the threshold was changed. This is then repeated for all three Minkowski Functional parameters. A binary logistic regression (BLR) was used to determine classification performance for each cohort split where only statistically significant parameters were entered into the regression – or all parameters if none returned as significant. A stepwise backwards Wald method was used, with a cut value of 0.5, and the final model was decided as the one with least number of parameters included.

Results

Results from the preliminary tests showed that statistically significant differences can be seen between all patient sub-groups except chemotherapy response. A summary of these results is presented in Table 2.

When determining how many orders were needed for polynomial analysis two measures of fit were examined, the adjusted r^2 and normalised-RMS values – which can be seen in Figs. 3 and 4. Both measures of performance improved as the number of terms is increased – with reduced change – and begin to plateau between 6th and 7th orders. These two results combined provide evidence for the use of 6th order polynomials to most accurately describe the data set and so this is what was chosen. Examples of the difference in rate of change of MF-values is illustrated in Fig. 5, where different curve shapes can clearly be seen for different patient groups.

Table 3 shows the results obtained from using 6th order polynomials to describe the changes in MF values as the threshold is raised. Statistically significant differences were found between TNBC status, biopsy grade, and lymphovascular invasion status sub-groups for all threshold

step values. No statistically significant results were found for chemotherapy response or nodal status for any modality. The number of significant findings changed as the number of threshold steps increased, however the variation in number of significant parameters is small and remained comparable across all methods. TNBC status returned the highest number of significant differences, with highly significant differences found for all numbers of thresholds used, an example of these results is given in Table 4.

Classification performance of 90.1% was found for TNBC status with sensitivity and specificity of 90.4% and 89.5% respectively. An ROC curve was plotted from the output of a binary logistic regression, seen in Fig. 6, returning an AUC of 0.935 (0.869 – 1.000 95% CI). Initial input parameters were chosen based on their significance during univariate analysis and a final model of 10 parameters (Perimeter 4-7, and Euler 1-6) was found to use the smallest amount of input parameters but remain significant. Classification performance of other groups are summarised as follows. Biopsy grade: 66.7%, (58.1% sensitivity and 74.0% specificity), AUC = 0.733 (0.633 – 0.833 95% CI) using a BLR with 4 parameters (Perimeter 3 and 5-7). Lymphovascular invasion: 68.4% (68.3% and 68.4%), AUC = 0.756 (0.648 – 0.864 95% CI) using a BLR with 5 parameters (Euler 1-5). Nodal status: 73.6% (73.3% and 73.9%), AUC = 0.782 (0.687 – 0.876 95% CI) using a BLR with 11 parameters (Area 4 and 5, Perimeter 1-7, and Euler 6 and 7). Chemotherapy response resulted in no significant results or regression model.

Discussion

It should be noted that two options exist for determining threshold levels; as although the same values ranging between 0 and 1 are chosen for each case, due to the non-uniform nature of pixel-intensities in MR scans the values of threshold levels do not relate to the same absolute pixel intensity of each image. “Local” thresholds allow for a greater range of binary images to

be created from full-ROI to blank images for all slices for all patients. “Global” thresholds allow for a more direct comparison between cases as each image is thresholded at a set pixel intensity as opposed to a relative one, however, this would result in a higher number of duplicate full-ROI or blank images as some scans fall well above/below certain pixel intensities. For this reason local thresholds were chosen in this study.

Nagarajan *et. al* (19) have concluded that there are diminishing returns when using higher numbers of binary images to perform texture analysis, and in other work it is common to use 20 or fewer thresholds (20, 21). Similar numbers of statistical difference were found when using 11, 51 and 101 threshold levels agreeing with previous work (19-21) that an increased number of threshold levels does not inherently result in greater differential power.

Second order polynomials were not included in this investigation as even the simplest curves (the area curves) would require a 3rd order polynomial to describe them based on visual inspection of their shape. The adjusted r^2 term was used as opposed to r^2 as it takes into account the addition of extra terms to create a closer fit.

Work by Larkin *et al.* demonstrated the ability of Minkowski Functionals to predict response to chemotherapy before visual effects are seen (20). This was done by comparing the change in MF values (ΔA , ΔU , and $\Delta \chi$) for scans taken before and after administration of chemotherapy drugs; in other words when chemotherapy treatment has already been decided upon and begun. This translates to a real world application of treatment monitoring/modification as opposed to true treatment prediction which would determine whether treatment should begin at all. The work conducted here used only pre-NAC scans and so is assessing if there is a detectable physiological difference between responsive and non-responsive tumours. No significant differences were found between responders and non-responders for any methodology used.

This new method of texture analysis has shown the ability to find a higher percentage of statistically significant indicators when differentiating between tumour statuses– particularly for TNBC status – than previous work by Ahmed *et al.* (4). Further, MFs have shown the ability to distinguish between lymphovascular invasion status, a task which is frequently unreported on but which holds important prognosis information (26).

When focusing on the results for TNBC status, Minkowski Functionals have demonstrated that there is a morphological difference between triple negative tumours and other tumour types. The number of significant findings – in Euler value especially – suggests a greater variance and heterogeneous appearance in TNBC cases. The heterogeneous appearance in images would explain the dip in Euler value (more holes) followed by a higher peak (more islands) than in other intrinsic subtype cases, creating a possibility of detecting triple negative tumours from an MRI scan when taken before commencement of NAC. This extra form of analysis would be non-intrusive as scans are already taken, and would provide more information for prognosis, affecting treatment planning, and overall patient care.

This study has a number of limitations. Firstly, as this was a single centre study a cohort of 100 patients was available; which although large when compared to similar studies (5,9,18,19), is a low population size when considering statistical power. This may have biased the results and also may have led to over fitted results. When using the binary logistic regression, the number of retained input parameters is very high for some models when compared to their respective group sizes (10 parameters for group sizes of 22 and 49 when looking at TNBC vs. Other intrinsic subtypes) which reduces the statistical power of the analysis to only looking at large effects (27). It should also be noted that this work constitutes a training set and as such the findings presented here require testing/validation on a new cohort of patients. Further, given the nature of the study the number of statistical tests performed for inclusion in regression

models is large; however, no correction for the number of tests performed was undertaken in this work.

Future work will hope to correct issues caused by small population sizes with the addition of new patients and possible inclusion of over sampling of existing data (28).

In Conclusion, Minkowski Functionals have already proved themselves to be able to distinguish between image homogeneity and heterogeneity (an established marker of malignancy), and the work presented in this paper demonstrates their ability to distinguish between patients in different cancer sub-groups. The performance of Minkowski Functionals remained comparable as the number of threshold steps was increased and so it can be considered that only a small number of thresholds are required for accurate analysis. Triple negative breast cancers were distinguishable when using Minkowski Functionals with a very high accuracy suggesting that there is an imaging abnormality about them when compared to other cancer types.

References

1. Cancer Research UK (2014), Cancer Stats report - Breast Cancer, Cancer Research UK.
2. Cancer Research UK, <http://www.cancerresearchuk.org/cancer-info/cancerstats/types/breast/mortality/uk-breast-cancer-mortality-statistics>, Accessed April 2015.
3. Atkins JJ, Appleton CM, Fisher CS, Gao F, Margenthaler JA. Which imaging modality is superior for prediction of response to neoadjuvant chemotherapy in patients with triple negative breast cancer? *Journal of oncology*. 2013 2013 (Epub 2013 Feb;2013:964863.
4. Ahmed A, Gibbs P, Pickles M, Turnbull L. Texture analysis in assessment and prediction of chemotherapy response in breast cancer. *Journal of magnetic resonance imaging : JMRI*. 2013 Jul;38(1):89-101.
5. Teruel JR, Heldahl MG, Goa PE, et al. Dynamic contrast-enhanced MRI texture analysis for pretreatment prediction of clinical and pathological response to neoadjuvant chemotherapy in patients with locally advanced breast cancer. *NMR Biomed*. 2014 Aug;27(8):887-96.
6. Kim H, Kim HH, Park JS, et al. Prediction of pathological complete response of breast cancer patients undergoing neoadjuvant chemotherapy: usefulness of breast MRI computer-aided detection. *Br J Radiol*. 2014 Nov;87(1043):7.
7. Yersal O, Barutca S. Biological subtypes of breast cancer: Prognostic and therapeutic implications. *World journal of clinical oncology*. 2014 2014 Aug;5(3):412-24.
8. Bertucci F, Finetti P, Birnbaum D. Basal Breast Cancer: A Complex and Deadly Molecular Subtype. *Current Molecular Medicine*. 2012 Jan;12(1):96-110.
9. Ansari MA, Astava VS, Sahoo BK, Kumar A. Status of Triple Negative Breast Cancer patients and its correlation with Vascularity in Indian scenario. *International Journal of General Medicine and Pharmacy*. 2014 31/12/2014;3(2):37-48.

10. Ovcaricek T, Frkovic SG, Matos E, Mozina B, Borstnar S. Triple negative breast cancer – prognostic factors and survival. *Radiol Oncol*. 2011 Mar;45(1):46-52.
11. Saslow D. American cancer society guidelines for breast screening with MRI as an adjunct to mammography (vol 57, pg 75, 2007). *CA-Cancer J Clin*. 2007 May-Jun;57(3):185-.
12. Morrow M, Waters J, Morris E. Breast Cancer 1 MRI for breast cancer screening, diagnosis, and treatment. *Lancet*. 2011 Nov;378(9805):1804-11.
13. Lord SJ, Lei W, Craft P, et al. A systematic review of the effectiveness of magnetic resonance imaging (MRI) as an addition to mammography and ultrasound in screening young women at high risk of breast cancer. *Eur J Cancer*. 2007 Sep;43(13):1905-17.
14. Wood C. Computer Aided Detection (CAD) for Breast MRI. *Technology in Cancer Research & Treatment*. 2005 February 1, 2005;4(1):49-53.
15. Connors RW, Trivedi MM, Harlow CA. Segmentation of a high-resolution urban scene using texture operators. *Computer Vision, Graphics, and Image Processing*. 1984 3//;25(3):273-310.
16. Boehm H, Fink C, Attenberger U, Becker C, Behr J, Reiser M. Automated classification of normal and pathologic pulmonary tissue by topological texture features extracted from multi-detector CT in 3D. *Eur Radiol*. 2008 Dec;18(12):2745-55.
17. Boehm HF, Schneider T, Buhmann-Kirchhoff SM, et al. Automated Classification of Breast Parenchymal Density: Topologic Analysis of X-Ray Attenuation Patterns Depicted with Digital Mammography. *American Journal of Roentgenology*. 2008 2008/12/01;191(6):W275-W82.
18. Boehm HF, Fischer T, Riosk D, Britsch S, Reiser M. Application of the Minkowski-Functionals for automated pattern classification of breast parenchyma depicted by digital mammography - art. no. 691522. In: Giger ML, Karssemeijer N, editors. *Medical*

- Imaging 2008: Computer-Aided Diagnosis, Pts 1 and 2. Bellingham: Spie-Int Soc Optical Engineering; 2008. p. 91522-.
19. Nagarajan MB, Huber MB, Schlossbauer T, Leinsinger G, Krol A, Wismuller A. Classification of small lesions in dynamic breast MRI: eliminating the need for precise lesion segmentation through spatio-temporal analysis of contrast enhancement. *Mach Vis Appl.* 2013 Oct;24(7):1371-81.
 20. Larkin TJ, Canuto HC, Kettunen MI, et al. Analysis of Image Heterogeneity Using 2D Minkowski Functionals Detects Tumor Responses to Treatment. *Magn Reson Med.* 2014 Jan;71(1):402-10.
 21. Canuto HC, McLachlan C, Kettunen MI, et al. Characterization of Image Heterogeneity Using 2D Minkowski Functionals Increases the Sensitivity of Detection of a Targeted MRI Contrast Agent. *Magn Reson Med.* 2009 May;61(5):1218-24.
 22. Park JO, Lee SI, Song SY, et al. Measuring response in solid tumors: Comparison of RECIST and WHO response criteria. *Japanese Journal of Clinical Oncology.* 2003 Oct;33(10):533-7.
 23. Hayes DF, Isaacs C, Stearns V. Prognostic factors in breast cancer: Current and new predictors of metastasis. *Journal of Mammary Gland Biology and Neoplasia.* 2001 Oct;6(4):375-92.
 24. Haybittle JL, Blamey RW, Elston CW, et al. A PROGNOSTIC INDEX IN PRIMARY BREAST-CANCER. *British Journal of Cancer.* 1982;45(3):361-6.
 25. Parker JS, Mullins M, Cheang MCU, et al. Supervised Risk Predictor of Breast Cancer Based on Intrinsic Subtypes. *J Clin Oncol.* 2009 Mar;27(8):1160-7.
 26. Mohammed Z, McMillan D, Edwards J, et al. The relationship between lymphovascular invasion and angiogenesis, hormone receptors, cell proliferation and survival in patients

with primary operable invasive ductal breast cancer. *BMC Clinical Pathology*.

2013;13(1):31.

27. Altman DG. *Practical statistics for medical research*: Chapman and Hall; 1990.
28. Chawla NV, Bowyer KW, Hall LO, Kegelmeyer WP. SMOTE: Synthetic minority over-sampling technique. *J Artif Intell Res*. 2002;16:321-57.

Table 1

Breakdown of patient cohort

	Number of Cases	% (of known)	Data Missing
Age			-
<45	30	30	
>=45	70	70	
Tumour Type			6
NST	37	39	
Ductal	47	50	
Lobular	9	10	
Unknown	1	1	
NAC Treatment			6
ECT	59 (73*)	63 (78*)	
NTT1	7 (8*)	7 (9*)	
NTT2	8	9	
FEC	1	1	
EC	3	3	
C	1	1	
Biopsy Grade			7
Grade 1/2	38	41	
Grade 3	55	59	
Intrinsic Subtype Status			29
Triple Negative	22	31	
All Other	49	69	
Nodal Status			9
+ve	46	51	
-ve	45	49	
Chemotherapy Response			11
Partial Responder	40	45	
Non Responder	49	55	
Lymphovascular Invasion Status			21
+ve	32	41	
-ve	47	59	

* Indicates a modified treatment course. NST: No Specific Type. NAC Treatment codes, E: Epirubicin, C: Cyclophosphamide, T: Taxotere, F: Fluorouracil, NTT1: EC and Paxlitaxel, NTT2: EC, Paxlitaxel and Gemcitabine.

Table 2

Summary of statistically significant differences ($p < 0.05$) found between of patient sub-groups.

	TNBC Status	Biopsy Grade	Nodal Status	Lymphovascular Invasion Status	Chemotherapy Response
Area	7	7	0	2	0
Perimeter	7	5	4	3	0
Euler	1	3	5	9	0
Total	15	15	9	14	0

Table 3

Comparison of the total number significant differences ($p < 0.05$) for different image processing methodologies, using 6th order polynomials, on 1 minute post-contrast images, with 3 texture parameters. P-values were calculated using Mann-Whitney U-tests.

	11 thresholds	51 thresholds	101 thresholds
TNBC Status	11	12	11
Biopsy Grade	1	1	1
Nodal Status	0	0	0
Lymphovascular Invasion	7	8	9
Chemotherapy Response	0	0	0

Table 4

Comparison of 6th order polynomials terms between triple negative breast cancer and other intrinsic subtype patients; calculated from MF values taken from 1 minute post-contrast images.

Texture Parameter	Mean \pm Standard Deviation		p-value
	TNBC	All Others	
Area 1 ($\times 10^{-5}$)	-1.80 \pm 2.64	-0.02 \pm 3.43	0.039
Area 2 ($\times 10^{-4}$)	6.53 \pm 9.27	1.12 \pm 11.57	0.071
Area 3 ($\times 10^{-3}$)	-8.54 \pm 12.59	-2.56 \pm 14.81	0.126
Area 4 ($\times 10^{-2}$)	4.94 \pm 8.26	1.92 \pm 9.09	0.248
Area 5 ($\times 10^{-1}$)	-1.41 \pm 2.66	0.64 \pm 2.79	0.291
Area 6 ($\times 10^{-1}$)	1.87 \pm 3.87	0.96 \pm 0.18	0.326
Area 7 ($\times 10^{-1}$)	0.91 \pm 0.19	0.95 \pm 0.20	0.364
Perimeter 1 ($\times 10^{-5}$)	1.38 \pm 6.91	3.54 \pm 5.96	0.238
Perimeter 2 ($\times 10^{-3}$)	-0.29 \pm 2.40	-1.20 \pm 2.07	0.149
Perimeter 3 ($\times 10^{-2}$)	0.14 \pm 3.15	1.53 \pm 2.76	0.098
Perimeter 4 ($\times 10^{-1}$)	0.04 \pm 1.97	-0.94 \pm 1.76	0.045
Perimeter 5 ($\times 10^{-1}$)	0.34 \pm 6.07	2.90 \pm 5.55	0.030
Perimeter 6 ($\times 10^{-1}$)	0.60 \pm 8.58	-4.14 \pm 8.06	0.026
Perimeter 7	0.73 \pm 0.47	1.09 \pm 0.36	0.001
Euler 1 ($\times 10^{-4}$)	6.47 \pm 18.18	-3.50 \pm 10.17	0.007
Euler 2 ($\times 10^{-2}$)	-2.34 \pm 6.43	1.00 \pm 3.48	0.008
Euler 3 ($\times 10^{-1}$)	3.08 \pm 8.83	-1.12 \pm 4.56	0.012
Euler 4	-1.81 \pm 5.93	0.64 \pm 2.90	0.014
Euler 5	4.91 \pm 20.02	-1.30 \pm 9.20	0.019
Euler 6	-6.10 \pm 30.72	2.67 \pm 13.43	0.033
Euler 7	4.60 \pm 15.98	0.63 \pm 7.21	0.060

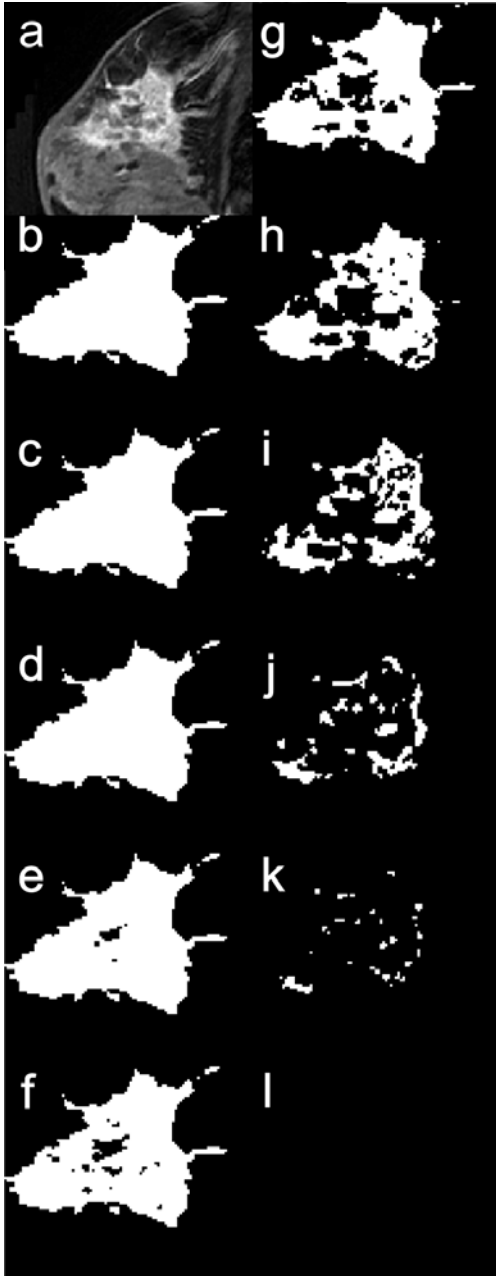


Figure 1: Demonstration of lesion segmentation, and binary image creation. The original T1w image (a) is segmented and then turned into binary images (b-l). Image (b) represent a threshold of 0.0 and so is the entire ROI, while image (l) represents a threshold of 1.0, and is thus blank.

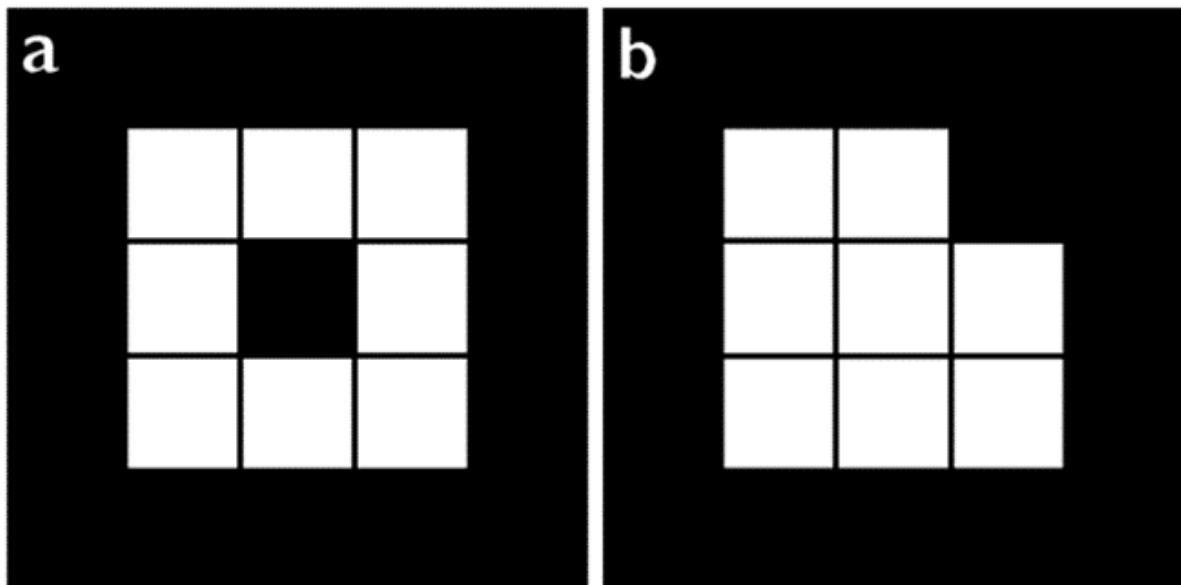


Figure 2: A comparison of MF values for examples of a (a) ‘ring’ and a (b) ‘block’ image, both made up of 8 white pixels. Image (a) has counting stats of $n_s = 8$, $n_e = 24$, and $n_v = 16$ giving MF values of $A = 8$, $U = 16$, and $\chi = 0$; and image (b) $n_s = 8$, $n_e = 22$, and $n_v = 15$, resulting in $A = 8$, $U = 12$, and $\chi = 1$.

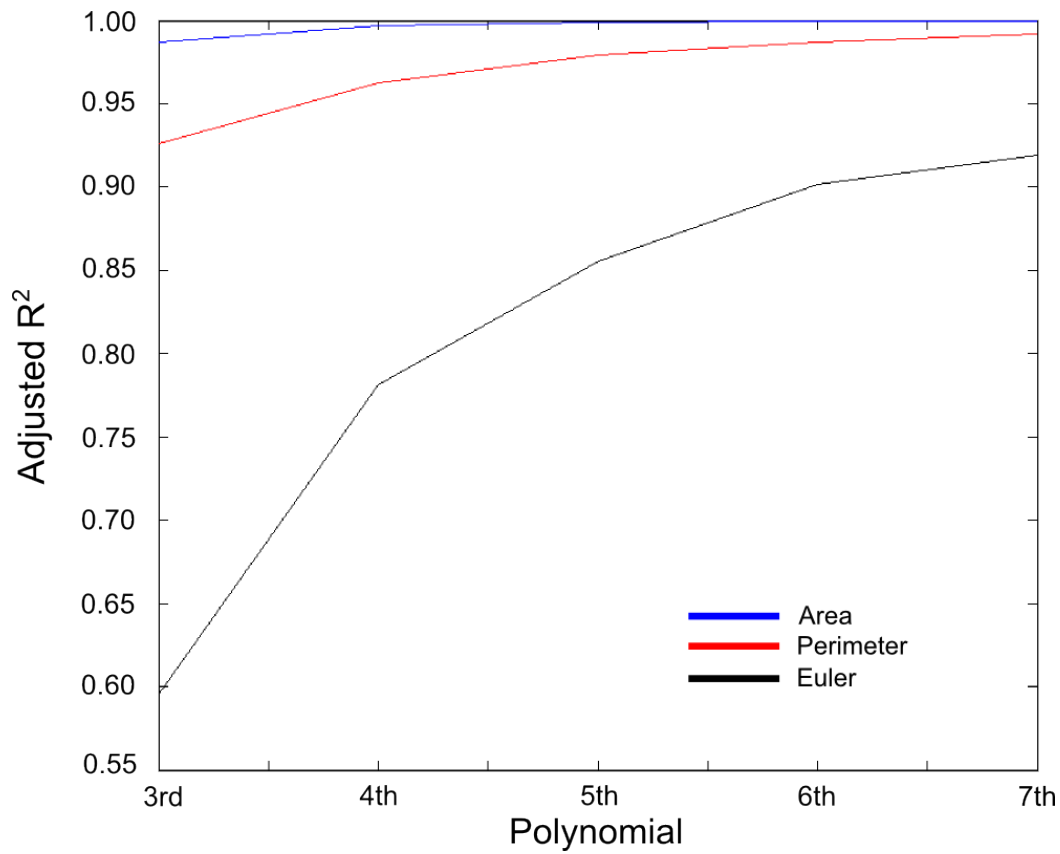


Figure 3: Visualisation of adjusted R^2 values for the three Minkowski Functionals comparing between 3rd, 4th, 5th, 6th and 7th order polynomials. The analysis performance increases as order of polynomials increases, beginning to plateau between 6th and 7th orders.

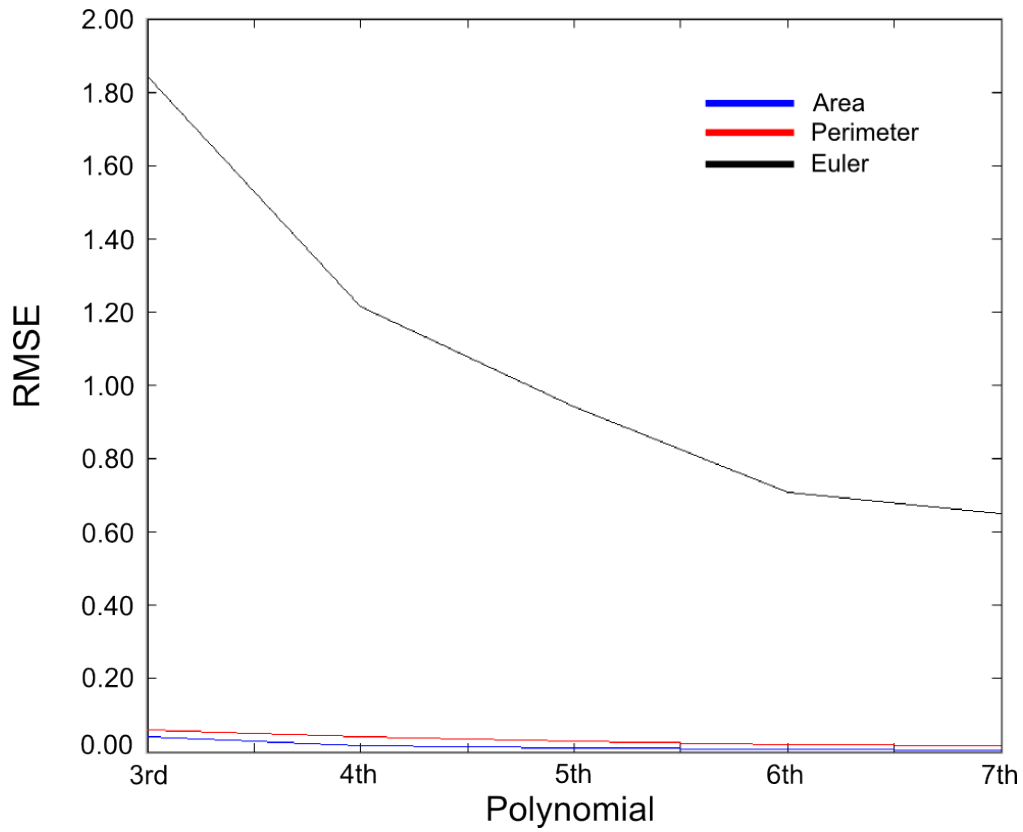


Figure 4: Visualisation of the route-mean-square error (RMSE) for the three Minkowski Functionals comparing between 3rd, 4th, 5th, 6th and 7th order polynomials. Only Euler value experiences significant change, decreasing as order is increased and plateauing between 6th and 7th order polynomials.

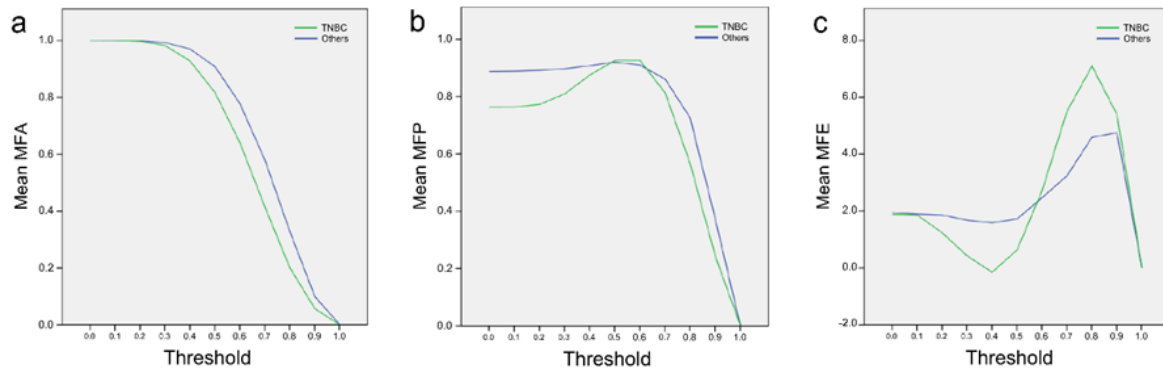


Figure 5: A comparison between the rate of change of MF values for (a) Area, (b) Perimeter, and (c) Euler value, for all Triple Negative (TNBC) and “Other” intrinsic subtype patients. The different parameter variations over threshold level are clear for each parameter.

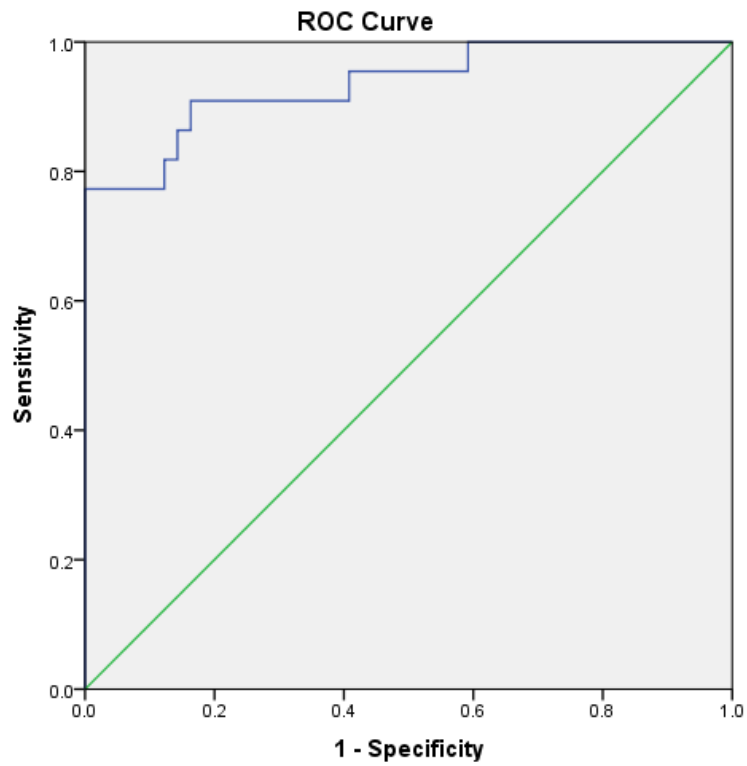


Figure 6: ROC analysis curve for binary logistic regression predictive factors for TNBC vs all others. AUC = 0.935 (0.869 – 1.000 95% C.I.) with p-value < 0.0001.



Figure 7: A comparison between Triple Negative (TNBC) and “Other” intrinsic subtype status breast cancer tumours as analysed using Minkowski Functionals. Both tumours are grade III and of No Specific Type (NST), and images are grouped into columns of identical threshold levels.